

PRIMER VECTOR BASED OPTIMAL GUIDANCE FOR ORBITAL TRANSFERS IN CISELUNAR ENVIRONMENT

Gabriele Gemignani⁽¹⁾, Giordana Bucchioni⁽²⁾, Stéphanie Lizy-Destrez⁽³⁾, Mario Innocenti⁽⁴⁾

⁽¹⁾*University of Pisa, Largo Lucio Lazzarino 2, g.gemignani11@studenti.unipi.it*

⁽²⁾*University of Pisa, Largo Lucio Lazzarino 2, giordana.bucchioni@unipi.it*

⁽³⁾*ISAE-SUPAERO, Avenue Édouard-Belin 10, stephanie.lizy-destrez@isae.fr*

⁽⁴⁾*University of Pisa, Largo Lucio Lazzarino 2, mario.innocenti@unipi.it*

ABSTRACT

Spacecraft Trajectory Design, and more precisely the minimization of fuel needed in space operations, is a topic that has increasingly attracted more interest, due to the desire of improving the efficiency of future space missions. The current investigation is inserted in this context, since it aims at providing a full optimization algorithm for fixed-time orbital transfers in the Circular Restricted Three Body Problem dynamic framework. Primer Vector theory is employed to assess optimality and provide a criterion to decrease the transfer cost by inserting intermediate impulsive manoeuvres along the trajectory. Numerical ad-hoc methods are first exploited to guess a reasonable 2-impulses transfer and estimate the Time Of Flight, this kept constant for the rest of the process. Tests are performed on transfers between Earth-Moon Halo orbits, which have been targeted by NASA as possible parking spots in future Moon missions, showing the results obtained in terms of fuel saving and optimality achievness.

1 INTRODUCTION

The ongoing interest in returning to the Moon and exploring the outer deep space finds evidence in the recent NASA Artemis program [1]. The plan originally scheduled is the permanent establishment, by the end of 2024, of a Lunar Gateway Station (or simply called Gateway) orbiting onto a Near Rectilinear Halo Orbit (NRHO), a subfamily of the Halo orbits in the Earth-Moon system [2]. This family of orbits was chosen due to particularly favourable stability and eclipsing avoidance properties, both factors bringing advantages in managing the energy resources available for the entire mission [3]. In this context of increasing interest for the space field, a large amount of research works has been focusing on spacecraft trajectory optimization. Minimizing the fuel brought on board is effectively a realistic goal which will help find more affordable paths through the outer space, in the attempt of exploring and possibly colonizing it with repeated missions in the next decades. Among the space operations with low-energy requirements, orbital transfer is indeed one of the most direct and typical applications, also referred to as phasing ([4], [5]).

When dealing with spacecraft trajectory optimization, separate choices are equally exploitable. The first distinction to make regards the mathematical model adopted to describe the space environment. It is known since Newton's epoch that a body in space moves under the gravitational attraction caused by all the celestial bodies surrounding it. What distinguishes one model from the other is the level of accuracy, which is translated in considering just 2 bodies in Newton's gravitational law, the Restricted Two Body Problem (R2BP) [6], to an arbitrary large number N , the N -body Problem [7]. The more

accurate the model, the more complex it is to analyse the system and to consequently synthesize an optimal control. A reasonable compromise often used, at least as a preliminary study, is the Circular Restricted Three Body Problem (CR3BP), which accounts for two dominant celestial bodies plus an additional one with negligible influence [8].

Another difference found inside trajectory optimization studies consists of the propulsion's nature. When the thrust is assumed as a continuous variable, the optimization is low-thrust and the Equations of Motion (EOMs) must consider the contribute of the input acceleration vector, which can act at any time during the propagation [9]. On the contrary, if propulsion acts only at discrete times and its duration is very short if compared to the mission's temporal arc, then the optimization is high-thrust and the EOMs only include the natural gravitational force. The high-thrust model is very often a reasonable assumption, not only due to the technological limitations of modern engines, but also because of the major simplicity in designing analytical expressions for high-thrust control laws.

Historically, another distinction is made based on the method employed to solve the optimization problem: the direct and the indirect methods [10]. While the direct methods approach the problem via some non-linear programming technique after discretization of the design variables, the indirect methods are based on the well-known optimal control theory [11]. Among the indirect methods, Lawden's Primer Vector (PV) theory [12] has turned out to be a powerful tool to assess optimality in Aerospace applications, as demonstrated by several existing works related to the optimization of both low [13] and high-thrust [14] transfers in CR3BP environment.

An indirect high-thrust optimization algorithm for fixed-time orbital transfers in CR3BP framework is presented in the current investigation. The low-energy fuel injection strategy is generated through the insertion of an arbitrary number of intermediate impulses along the path, by employing both PV and non-linear optimization theory. The algorithm is implemented as additional module of the already existing Sun-Earth-Moon python (SEMPy) library [15], a software tool for studies in non-keplerian environments developed and maintained at ISAE-SUPAERO, Toulouse, France. With respect to previous similar works [16], this paper gives a detailed description of the structure of the algorithm proposed and combines it with numerical initial guess determination methods in order to validate it in a large set of applications. The topics are organized as follow: the second section poses the mathematical basis needed in the development of this work, from the CR3BP dynamic model adopted to Lawden's PV theory, which represents the core of the optimization process, to the Multiple Shooting (MS) numerical method to build trajectories satisfying specific constraints; the third section describes some implementation details for the sake of reproducibility of this work's results, these ones being then illustrated, for Halo-Halo transfer cases, and deeply assessed in the fourth section; the fifth and final section of the paper draws the conclusions, putting the emphasis on the points of strength and weakness of the present algorithm and explaining what should be improved in future investigations before it could realistically become a useful mission design tool.

2 METHODOLOGY

In the rest of the paper, scalar quantities are indicated with non-bold letters, while multi-dimensional quantities, such as vectors and matrices, with bold font. This means, for example, that we will refer to the velocity vector as \mathbf{v} , while its norm will be denoted with v .

2.1 Circular Restricted Three Body Problem

The spacecraft is modelled as a particle of mass m which moves under a gravitational potential caused by two primary bodies m_1 and m_2 , with $m \ll m_2 < m_1$. Since m is considerably minor than the other two masses, its effect on the overall gravitational field is negligible. The mass parameter of the

CR3BP framework is defined as:

$$\mu = \frac{m_2}{m_1 + m_2} \in (0, 1) \quad (1)$$

To remove any explicit dependence from time, the EOMs are conveniently derived in a rotating reference frame, illustrated, together with the fixed inertial one, in Fig.1. Here, the x -axis is always aligned with the two primary bodies, which rotate at constant angular speed Ω around the primaries' barycenter, located in the frame origin O_G , and the z -axis points in the direction of the system's angular momentum (with the y -axis to complete the right-handed triad). Additionally, position and times are normalized respectively per L , the distance between the primaries, and per $T_c/2\pi$, where T_c refers to the orbital period of the circular motion. From $\Omega = 2\pi/T_c$, it also follows that the normalized angular speed is unitary.

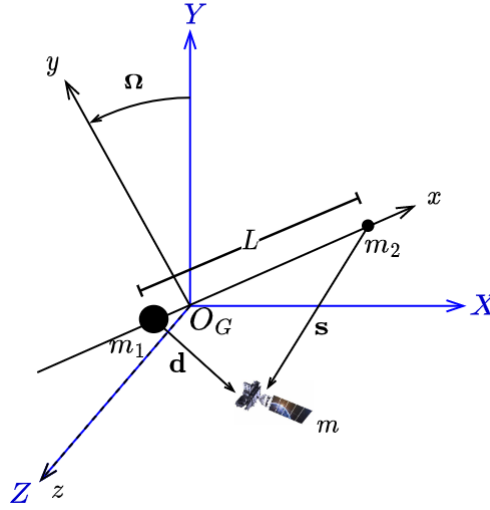


Figure 1: Dynamic framework: in blue the fixed inertial frame, in black the rotating frame

Denoted with $\mathbf{x} = [\mathbf{r} \ \mathbf{v}]^T = [x \ y \ z \ v_x \ v_y \ v_z]^T$ the spacecraft's state expressed in the normalized rotating frame, writing the kinetic and potential energy and passing by the Euler-Lagrange equation one obtains [8]:

$$\dot{\mathbf{x}} = \mathbf{f}(\mathbf{x}) \begin{cases} \dot{\mathbf{r}} = \mathbf{v} \\ \dot{v}_x = x + 2v_y - (1 - \mu) \frac{(x+\mu)}{d^3} - \mu \frac{(x-1+\mu)}{s^3} \\ \dot{v}_y = -2v_x + y - (1 - \mu) \frac{y}{d^3} - \mu \frac{y}{s^3} \\ \dot{v}_z = -(1 - \mu) \frac{z}{d^3} - \mu \frac{z}{s^3} \end{cases} \quad (2)$$

The EOMs are characterized by high non-linearity and a third-order singularity in $d = 0$ and $s = 0$, namely in correspondence of the primary bodies, being d and s respectively the distances from m_1 and m_2 . Moreover, a study on the equilibria of the dynamic system described by Eq.2 yields 5 points, the so-called Lagrange points $L_i, i = 1 \dots 5$, around which some interesting periodic solutions arise starting from the linearized dynamic (such as the Halo orbits mentioned in the introduction to this work) [17].

A first-order sensitivity analysis leads to the definition of the State Transition Matrix (STM), defined as a matrix $\Phi_{t,t_0} \in \mathbb{R}^{6 \times 6}$ obeying the matricial differential equation:

$$\dot{\Phi}_{t,t_0} = \frac{\partial \mathbf{f}(\mathbf{x})}{\partial \mathbf{x}} \Phi_{t,t_0} \quad \Phi_{t_0,t_0} = \mathbf{I}_{6 \times 6} \quad (3)$$

The STM relates a perturbation in the state at a generic time t with the initial perturbation at time t_0 through the equation:

$$\begin{bmatrix} \delta \mathbf{r}_t \\ \delta \mathbf{v}_t \end{bmatrix} = \Phi_{t,t_0} \begin{bmatrix} \delta \mathbf{r}_0 \\ \delta \mathbf{v}_0 \end{bmatrix} = \begin{bmatrix} \mathbf{A}_{t,t_0} & \mathbf{B}_{t,t_0} \\ \mathbf{C}_{t,t_0} & \mathbf{D}_{t,t_0} \end{bmatrix} \begin{bmatrix} \delta \mathbf{r}_0 \\ \delta \mathbf{v}_0 \end{bmatrix} \quad (4)$$

2.2 Primer Vector Theory

The orbital transfer is optimized in this work through the insertion of intermediate impulsive maneuvers along the path, under high-thrust hypothesis. Assuming to have a set of N nodes, modelling the points in the space where an instantaneous change of velocity $\Delta \mathbf{v}$ can occur, the optimization problem is translated in the minimization of the cost function:

$$J_N = \sum_{i=0}^{N-1} \|\Delta \mathbf{v}_i\| = \sum_{i=0}^{N-1} \Delta v_i \quad (5)$$

The number of total nodes N is a design variable of the optimization problem. While the first and final node are constant and specified as boundary constraints of the problem, the intermediate ones are selected based on an indirect optimization process which exploits the well-consolidated PV theory [12]. Given two consecutive nodes (\mathbf{x}_i, t_i) and $(\mathbf{x}_{i+1}, t_{i+1})$ previously connected, the PV and its derivative at a generic time t , with $t_i < t < t_{i+1}$, can be computed as [18]:

$$\begin{aligned} \mathbf{p}_t &= (\mathbf{A}_{t,i} - \mathbf{B}_{t,i} \mathbf{B}_{i+1,i}^{-1} \mathbf{A}_{i+1,i}) \frac{\Delta \mathbf{v}_i}{\Delta v_i} + \mathbf{B}_{t,i} \mathbf{B}_{i+1,i}^{-1} \frac{\Delta \mathbf{v}_{i+1}}{\Delta v_{i+1}} \\ \dot{\mathbf{p}}_t &= (\mathbf{C}_{t,i} - \mathbf{D}_{t,i} \mathbf{B}_{i+1,i}^{-1} \mathbf{A}_{i+1,i}) \frac{\Delta \mathbf{v}_i}{\Delta v_i} + \mathbf{D}_{t,i} \mathbf{B}_{i+1,i}^{-1} \frac{\Delta \mathbf{v}_{i+1}}{\Delta v_{i+1}} \end{aligned} \quad (6)$$

Putting together the results obtained with Eq.6 for each pair of adjacent nodes, the whole PV history along the trajectory is derived. Then, the local optimality can be assessed based on the satisfactory of Lawden's necessary conditions:

1. \mathbf{p} and $\dot{\mathbf{p}}$ must be continuous everywhere.
2. $p = \|\mathbf{p}\| \leq 1$ along the whole trajectory, with $p = 1$ at those times in which an impulse occurs.
3. When $p = 1$, the PV is a unit vector pointing in the direction of the optimal thrust.
4. At the intermediate impulses, $\dot{p} = \frac{d}{dt} \|\mathbf{p}\| = 0$.

In case $\|\mathbf{p}\| > 1$ during a specific time interval, the total transfer cost can be decreased by adding a new node at a proper time and then displacing its position to initialize a velocity discontinuity. Computing the difference in the total cost result of the perturbation of a nominal trajectory, the maximum decrease in cost is proved to be obtained if the intermediate node is first initialized onto the current path at the time of maximum PV magnitude \mathbf{p}_m , say (\mathbf{x}_m, t_m) , and then its position is perturbed of the quantity [19]:

$$\delta \mathbf{r}_m = \beta (-\mathbf{B}_{i+1,m}^{-1} \mathbf{A}_{i+1,m} - \mathbf{D}_{m,i} \mathbf{B}_{m,i}^{-1})^{-1} \frac{\mathbf{P}_m}{p_m} \quad (7)$$

At this point, computing the PV again with Eq.6, the fourth Lawden's law is usually not verified, as in the process of derivation of Eq.7 the derivative is not taken into account. However, the position \mathbf{r}_i and time t_i of all the intermediate impulses can subsequently be optimized thanks to a gradient-based non-linear minimization process, exploiting the analytical knowledge of the first derivative ∇J :

$$\begin{aligned} \frac{\partial J_N}{\partial \mathbf{r}_i} &= \dot{\mathbf{p}}_i^+ - \dot{\mathbf{p}}_i^- \\ \frac{\partial J_N}{\partial t_i} &= \dot{\mathbf{p}}_i^- \cdot \mathbf{v}_i^- - \dot{\mathbf{p}}_i^+ \cdot \mathbf{v}_i^+ \end{aligned} \quad (8)$$

where the superscript notation distinguishes the quantities immediately before (-) and after (+) the velocity discontinuity. The convergence towards the stationary point of J implies the satisfactory of the zero-derivative condition at the intermediate impulses, but not necessarily the one regarding the PV magnitude. The whole process of initialization of a new node, displacement of its position and gradient-based optimization can nevertheless be iterated, until Lawden's necessary conditions of optimality are all verified. In the present work, the Broyden-Fletcher-Goldferb-Shanno (BFGS) method [20] is used, which means the design variable vector $\mathbf{k} = [\mathbf{r}_1, t_1, \dots, \mathbf{r}_{N-2}, t_{N-2}]$ moves at each iteration according to the update expression:

$$\mathbf{k} = \mathbf{k} - \alpha \mathbf{H} \nabla J \quad (9)$$

where α is the perturbation's step length and is selected via a Wolfe Line Search (WLS) [20], while \mathbf{H} is the approximate inverse Hessian computed by the method at each step in order to achieve super-linear convergence speed under certain regularity assumptions.

2.3 Multiple Shooting

The BFGS optimization process requires the evaluation of the cost function given by Eq.5 in several different configurations of the intermediate manoeuvres. In order to compute the quantity $\|\Delta \mathbf{v}_i\| = \|\mathbf{v}_i^+ - \mathbf{v}_i^-\|$ for each i with enough precision, one has to first ensure the position continuity between the propagated state from the node before and the node after, both at the unique time t_i , namely $\mathbf{r}_i^- = \mathbf{r}_i^+$. As no exact solution to this problem has been found yet, the typical resolution procedure consists of a numerical method known in literature as Multiple Shooting (MS) [21] and depicted,

for the application at hand, in Fig.2. Here, the initial and final points are determined by the boundary constraints of the transfer, while the intermediate nodes are guided in position and time by the gradient of Eq.8. From these considerations, it follows that the only unconstrained variables, whose value must be found such that the spacecraft does not jump in position along the path, are the velocities at each node. For the moment, the propagation occurs directly between two consecutive nodes, resulting in a single arc, from which the MS method assumes the form of its simplest variant, also called Single Shooting (SS).

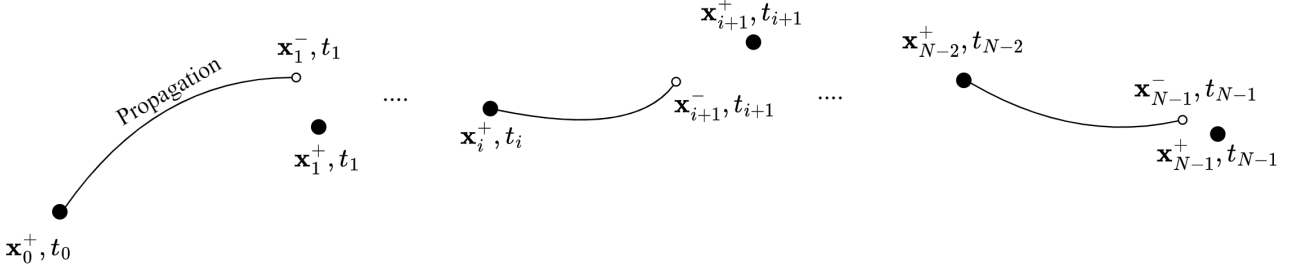


Figure 2: Single Shooting procedure for a set of N nodes

Defining the vector of variables and constraints as:

$$\begin{aligned} \mathbf{z} &= [\mathbf{v}_0^+, \dots, \mathbf{v}_{N-2}^+] \in \mathbb{R}^{3 \times (N-1)} \\ \mathbf{g}(\mathbf{z}) &= [\mathbf{r}_1^- - \mathbf{r}_1^+, \dots, \mathbf{r}_{N-1}^- - \mathbf{r}_{N-1}^+] \in \mathbb{R}^{3 \times (N-1)} \end{aligned} \quad (10)$$

the system of equations $\mathbf{g}(\mathbf{z}) = \mathbf{0}$ has a unique solution, which can be found via any multi-variable Newton-like root-finding method (for example Levenberg-Marquardt to enlarge the local domain of convergence [22]). The first derivative is a sparse matrix composed by sub-blocks of the STM and identity matrices, as one can easily verify taking into account Eq.4.

Sometimes the SS method has convergence issues due to mainly two reasons: inappropriate choice of the initial guess or high sensitivity related to the ill-conditioned Jacobian matrix. The first factor is a typical problem to deal with in every local convergence domain numerical procedure. In the present work, the best effort initial guess for the computation of the perturbed trajectory is represented by the current one, relying on the small perturbations assumption. As regards the sensitivity, it rises especially in the proximity of the CR3BP singularities or for excessively long integrations. A practical strategy to try to solve this problem is to split the propagation between consecutive nodes in multiple segments (from which the generalization to the MS method), initializing some additional fictitious nodes onto each propagated arc and adding them to the root-finding problem defined in Eq.10. To do so, it is necessary to point out that, since these newly added points have no physical meaning but rather just represent a numerical aid, the whole state's continuity must be ensured for them. Additionally, their position is free to change together with their velocity, while their time is kept fixed once initialized equally spaced one from the other. Because of these considerations, the system maintains the property of square dimension, and consequently a unique solution is searched even with in the most general MS approach. Unfortunately, there is no theoretical rule regarding the number of fictitious nodes to insert along each arc; as the goal of this part of the algorithm is to successfully build a trajectory, several trials are made, starting from the simpler SS and eventually increasing the number of fictitious nodes in order to decrease the sensitivity and hopefully converge to the solution with the desired precision (which, in a double precision implementation, cannot be set lower than $\|\mathbf{g}\| < 10^{-13}$). For the rest of the work, we will refer to this part of the algorithm as simply MS, since it represents the most general case of building any trajectory, independently from whether fictitious nodes are inserted to decrease the sensitivity or not and how many of them.

3 IMPLEMENTATION

The whole project is built over SEMpy, an open-source python library (the GitLab public repository can found in [23]) developed and continuously updated by the space Advanced Concept Laboratory (SACLab) team at ISAE-SUPAERO [15]. It offers useful tools for mission design analysis in non-Keplerian environments, both for research and education purposes . Over the SEMpy layer, a high-thrust PV-based optimization algorithm for fixed-time orbital transfers in CR3BP dynamic framework was implemented, the scheme of which is reported in Alg.1.

Algorithm 1 PV-based Optimization of fixed-time orbital transfers in CR3BP framework

Input: CR3BP pair, departure and arrival orbit, departure and arrival position

$N \leftarrow 2$

Compute initial guess J_N

Compute PV

repeat

$m \leftarrow \arg \max \text{PV}$

 Initialize new node (\mathbf{r}_m, t_m)

$N \leftarrow N + 1$

 Compute $\delta \mathbf{r}_m$

$\mathbf{r}_m \leftarrow \mathbf{r}_m + \delta \mathbf{r}_m$

 Compute J_N and PV

 Gradient-based optimization

until Lawden's optimality laws are all verified

The first input to precise is obviously the pair of primary bodies aimed at studying, identified by the mass parameter of Eq.1 or by the characteristic length and time of the CR3BP normalized rotating frame, introduced in section 2 respectively as L and T_c . Then, the departure and arrival periodic orbits involved in the transfer are computed thanks to the orbit propagation module provided by SEMpy. The attribute fixed-time refers to the transfer time, also known as Time Of Flight (TOF), which is settled in the initial guess computation phase of the algorithm and then kept fixed for the whole optimization process. As for the initial and final node of the transfer, the ones located respectively onto the departure and arrival orbit, it holds that:

$$\begin{aligned} d\mathbf{r}_0^- &= \mathbf{v}_0^- dt_0 \\ d\mathbf{r}_{N-1}^+ &= \mathbf{v}_{N-1}^+ dt_{N-1} \end{aligned} \quad (11)$$

and since $dt_0 = dt_{N-1} = 0$, it follows that the departure and arrival positions are also constant once specified at the beginning of the algorithm as user-defined inputs. In that sense, the angle swept by the spacecraft with respect to the last passage by the periapsis, namely the point of an orbit closest to the primary body, is defined as:

$$\theta = \frac{t}{T} 360^\circ \in [0^\circ, 360^\circ) \quad (12)$$

with t the current time and T the orbit period. Eq.12 permits to completely characterize the initial and the final node of the transfer once selected the desired θ_d and θ_a on the corresponding orbit. The strategy adopted in this work for the determination of the TOF is based on the way the initial guess is computed. Since, unfortunately, no exact analytical 2-impulses solution exists in complex non-linear environments like the CR3BP, some ad-hoc MS-based methods are exploitable depending on the application at hand. The well-known Lambert solution to the R2BP [24] can be fed as initial trajectory to a MS correction procedure, even though most of the times it deviates considerably from the CR3BP dynamic, so that its output is often not reliable. Another commonly used approach in literature is the orbit chaining method [25], which has the advantage of being more faithful to the dynamic environment adopted but at the same time more restrictive regarding the set of transfers it can be applied on. Constraining the orbits involved in the transfer to belong to the same family in fact, the TOF can be first approximated as an average of the departure and arrival orbits' period, respectively T_d and T_a , weighted for the angle swept throughout the transfer:

$$TOF = \frac{|T_d - T_a|}{2} \begin{cases} (\theta_a - \theta_d)/360 & \theta_a > \theta_d \\ (\theta_a - \theta_d)/360 + 1 & \theta_a \leq \theta_d \end{cases} \quad (13)$$

Then, the orbits in between them can be exploited to build a reasonable initial guess with a shape similar to the one of the family itself. More specifically, an arbitrary number of nodes is positioned equally spaced onto the intermediate orbits and then connected via a MS procedure. If, on one hand, as a heuristic rule, one could take more intermediate orbits to mitigate the high sensitivity caused by longer transfers, it is equally true that the highly complex and unpredictable CR3BP environment makes it difficult to generalize this rule. For this reason, a trial-and-error approach is once again adopted, in a similar fashion of how described before for building the trajectories with the MS method during the gradient-based optimization.

Before showing the results obtained, it is worthy to evidence some algebraic manipulation that helped mitigating the possibly arising numerical issues. First, looking back at Eq.2, there is one significant difference between the CR3BP mathematical model and the real physical scenario: the singularities, which just consist of two points inside the EOMs, actually represent the centre of approximately spherical celestial bodies. Given this contrast, some limits must be enforced on the state space explorable by the BFGS optimization, to account for the fact that the spacecraft cannot pass arbitrarily close to the primaries, even though the mathematical model would technically allow that, otherwise it would crash onto them. Even though this will not avoid the singularities to occur but rather decrease their frequency, it is acceptable, in the current implementation, to fall within one of those cases from time to time and have irrelevant to the final result computational slowdowns.

It may happen sometimes, often when the perturbation in the nominal trajectory is greater than what is admissible from the first-order small perturbations analysis, that the MS procedure does not converge even if increasing the number of fictitious nodes in the middle. In those cases, the algorithm's performance can degrade notably, since the evaluation of Eq.5 is erroneous. Instead of accepting a gross level of precision, the current perturbation's step length α in Eq.9 is rejected and the WLS goes on. The simulations performed seemed to confirm that this choice, provided that such failure does not occur too often, does not irremediably affect the optimization procedure, since, following the rejection, a new reduced step length is tested, consequently getting closer to an admissible size of perturbation. Even in the unfortunate case that the WLS does not find an admissible step length in a certain BFGS iteration, the research is repeated after the approximate second derivative \mathbf{H} is reinitialized to a multiple of the identity matrix, cancelling possible estimation errors occurred throughout the process and making the direction of search $-\mathbf{H}\nabla J$ instantly closer to a more robust gradient-descent.

4 RESULTS

The optimization algorithm is tested on Earth-Moon Halo to Halo transfers, in order to prove its validity in a modern realistic context like NASA Artemis program. The arrival orbit is chosen as the L_2 southern 9:2 lunar synodic resonance NRHO (9 NRHO revolutions per 2 lunar months), whose properties are listed in Tab.1, originally designed to host the Gateway [26]. The periselene is the alternative name of the periapsis in case the spacecraft orbits around the Moon. The Jacobi constant C is an indicator of the orbit's energy integral of motion, according to the classical definition $C = -2E$, with E the mechanical energy in the normalized rotating frame [8].

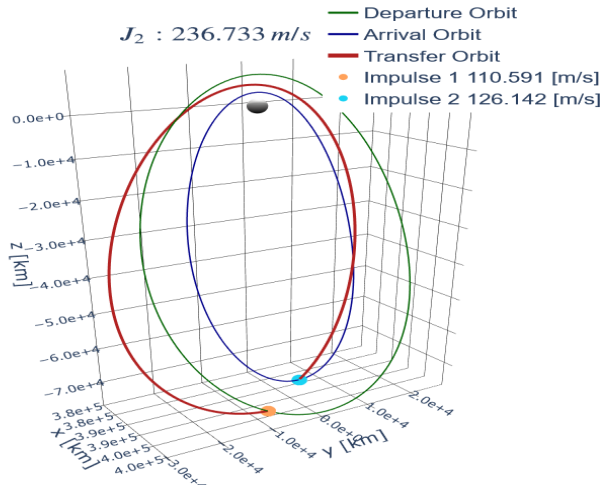
Table 1: Gateway orbit characteristics

Periselene Radius	$R_a = 3225.211$ km
Period	$T_a = 6.562$ days
Jacobi constant	$C_a = 3.058$

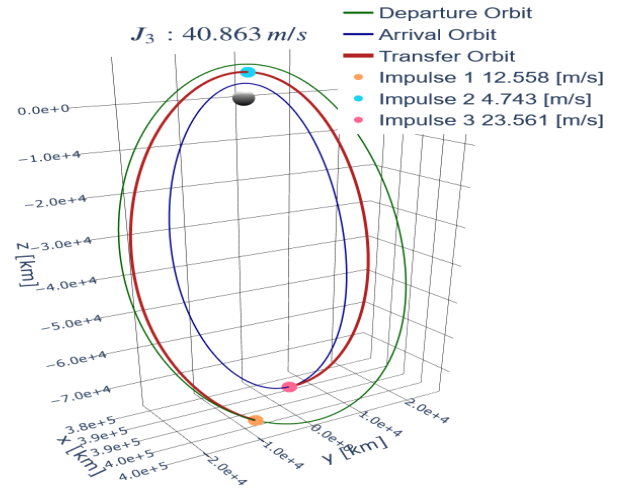
The examples reported in Fig.3-5 are cases of transfer involving the Gateway arrival orbit, associated with the properties in Tab.1, and a departure orbit still belonging to the L_2 southern NRHOs but with a period of $T_d = 1.2 T_a$. The orbit chaining method is used in this first test phase to first approximate the TOF via Eq.13 and then determine Halo-like shaped initial 2-impulses transfers, like the ones shown in Fig.3a, Fig.4a and Fig.5a. In Fig.3b, Fig.4b and Fig.5b instead the optimal N -impulses transfer is illustrated, with $N \geq 2$, result of the optimization algorithm described in Alg.1. Major fuel savings are always to relate to lower-quality initial guesses, as in Fig.3a and Fig.4a, while less expensive 2-impulses transfers, like the one in Fig.5a, are closer to the optimal solution and consequently have less margins of improvement. The fuel saving does not depend on the number of intermediate maneuvers added as a result of the optimization, rather on the TOF of the transfer. In fact, from the simulations it emerged that cases characterized by close departure and arrival states occur very rapidly, but at the expense of being more expensive and usually not optimizable according to PV theory. For more prolonged transfers, the opposite consideration holds, even if excessively long propagations must be avoided to prevent uncontrollable increases in the sensitivity and because, from a practical point of view, it is undesirable to have too high TOFs, especially in crewed missions.

Associated with Fig.3-5, Fig.6-8 report the PV trends in terms of PV magnitude and its approximate derivative, both for the initial and optimized case. The times at which an impulse occurs are underlined with an empty red circle in order to verify the satisfactory of Lawden's condition regarding whether the PV magnitude value at those times is unitary or not. The red star in each initial PV graph points out the magnitude's peak, which corresponds to the time at which a new impulse must be initialized according to PV theory. In case the 2-impulses initial guess turns out to be optimal, either because the transfer is effectively cheap or it is so unreasonable that is not optimizable, such red star is not present. Furthermore, even if the intermediate results (for example the 3 and 4-impulses PV related to Fig.7) are not shown due to lack of space, it is worthy to mention an interesting behaviour displayed by the algorithm. If on one hand the peak on the 2-impulses PV can generally be notably high, as it is for Fig.6a and Fig.8a, this feature becomes less and less evident as the algorithm proceeds. As immediate consequence, the algorithm achieves the largest fuel savings in the first steps, mainly passing from 2 to 3 impulses, rather than in the latest, where the transfers are semi-optimal due to the PV magnitude being barely greater than one.

The graphs of the optimized PV history also evidence the derivative value at the intermediate impulses time. As demanded by Lawden's fourth optimality criterion, these must be zero following the BFGS optimization procedure, as it can be proven taking the expression of the gradient of Eq.8 and equalling it to zero [18]. While in Fig.7b the condition is fully respected, some derivatives in Fig.6b and Fig.8b present small residuals, whose presence is due to two simple considerations: the first and most

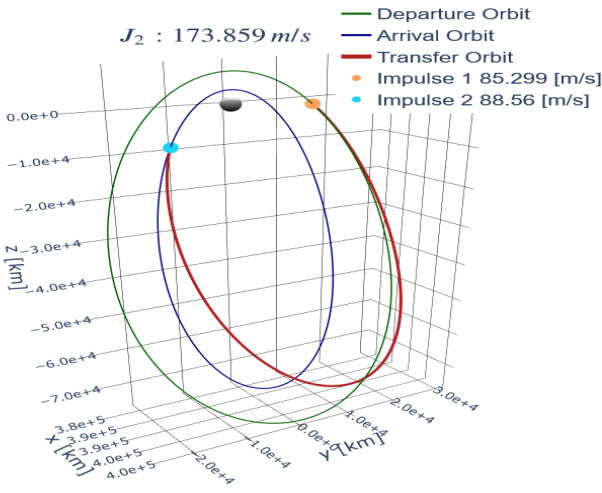


(a) 2-Impulses transfer

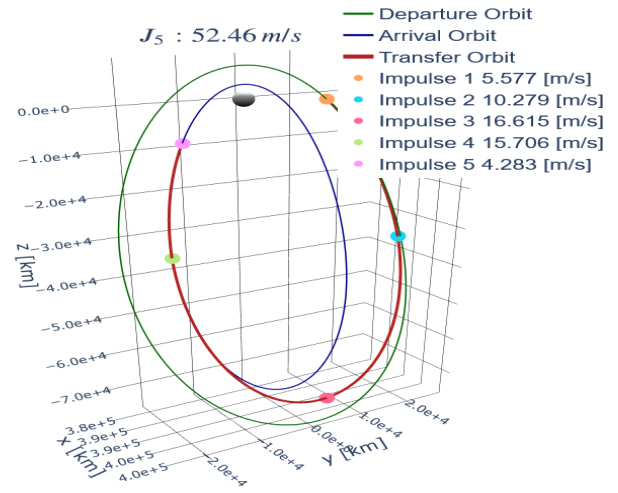


(b) 3-Impulses transfer

Figure 3: L_2 southern NRHO to Gateway transfer: $T_d = 1.2 T_a$, $\theta_d = 220^\circ$, $\theta_a = 180^\circ$

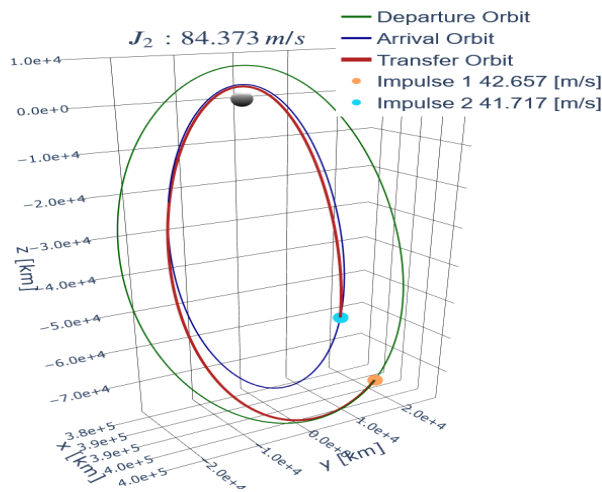


(a) 2-Impulses transfer

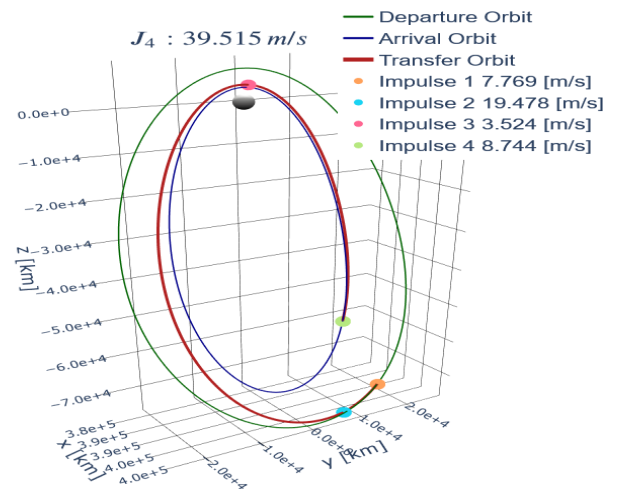


(b) 5-Impulses transfer

Figure 4: L_2 southern NRHO to Gateway transfer: $T_d = 1.2 T_a$, $\theta_d = 10^\circ$, $\theta_a = 350^\circ$

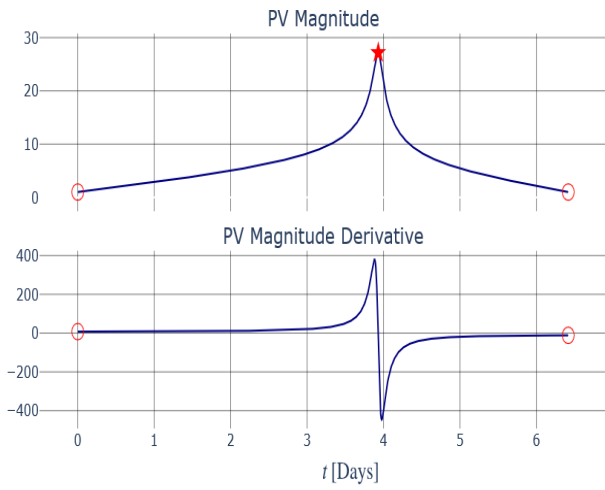


(a) 2-Impulses transfer

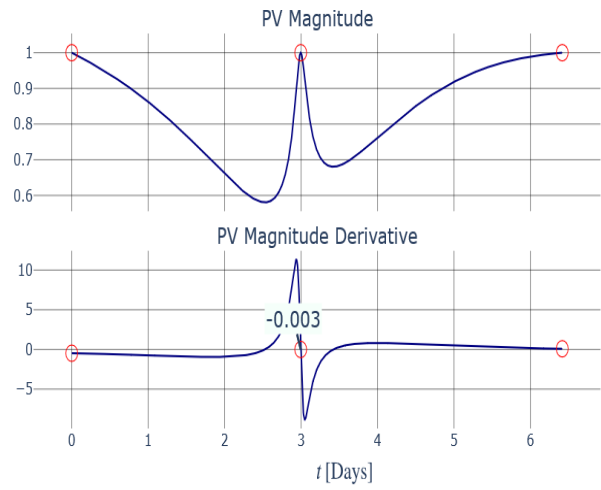


(b) 4-Impulses transfer

Figure 5: L_2 southern NRHO to Gateway transfer: $T_d = 1.2 T_a$, $\theta_d = 130^\circ$, $\theta_a = 90^\circ$

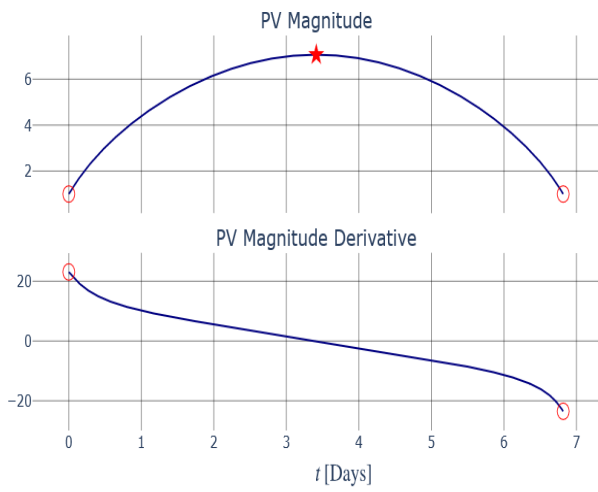


(a) 2-Impulses PV

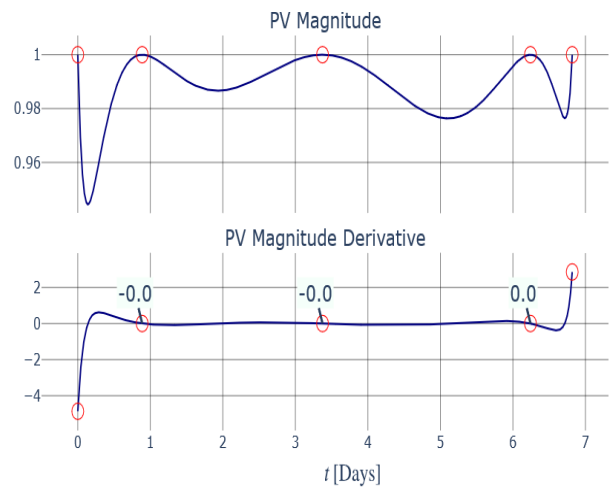


(b) 3-Impulses PV

Figure 6: L_2 southern NRHO to Gateway PV: $T_d = 1.2 T_a$, $\theta_d = 220^\circ$, $\theta_a = 180^\circ$

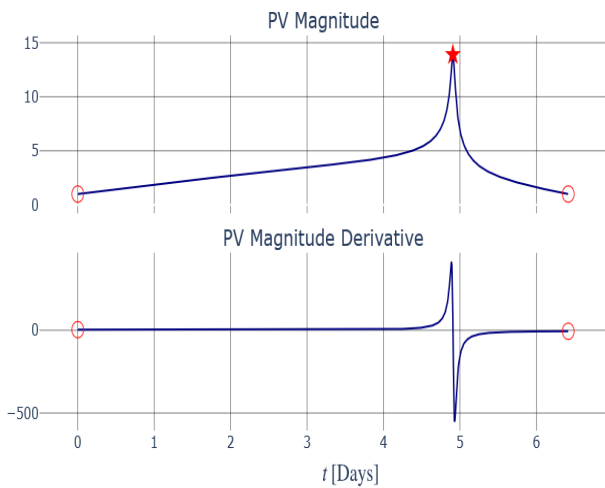


(a) 2-Impulses PV

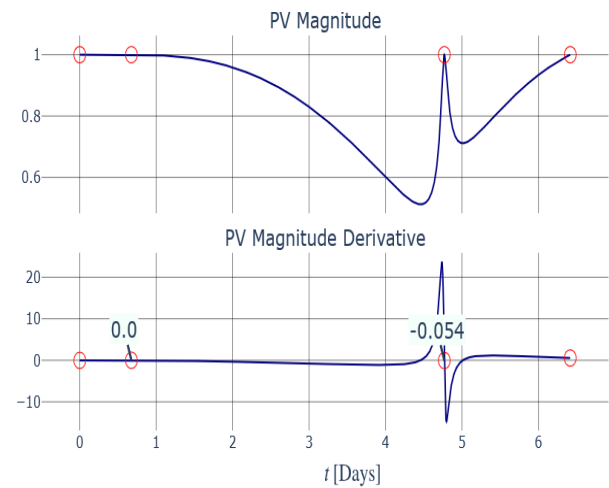


(b) 5-Impulses PV

Figure 7: L_2 southern NRHO to Gateway PV: $T_d = 1.2 T_a$, $\theta_d = 10^\circ$, $\theta_a = 350^\circ$



(a) 2-Impulses PV



(b) 4-Impulses PV

Figure 8: L_2 southern NRHO to Gateway PV: $T_d = 1.2 T_a$, $\theta_d = 130^\circ$, $\theta_a = 90^\circ$

important one is that the BFGS optimization is nested on the MS inner numerical method, so that due to machine precision its is limited to 5-6 digits after the comma; this limitation could be overcome passing to quadruple machine precision, in spite of course of much longer computational times. The other reason stands in the computation of the PV magnitude derivative itself, as it is performed with an approximate finite difference method [27], inevitably giving raise to tiny errors in the process. It must be noted though that too different from zero values of the derivatives are sign of an abnormal behaviour of the BFGS optimization and prevent the convergence towards the optimal solution.

In order to validate the method in multiple different scenarios, other simulations were performed with more distant orbits involved, for which the optimization is intuitively expected to have a lower convergence rate. Fig.9 and Fig.10 illustrate a case of transfer and the related PV history involving a more distant L_2 southern Halo departure orbit than the one seen in Fig.3-5, while Fig.11-Fig.12 show an example of transfer in which the departure orbit is a L_1 northern Halo with the same Jacobi constant of the Gateway arrival orbit. As in this last example the two orbits belong to different families, the orbit chaining initial guess method is not exploitable and the MS-corrected Lambert solver must be used, with a TOF set to 8 days according to a previous work about optimal Halo-Halo phasing [28].

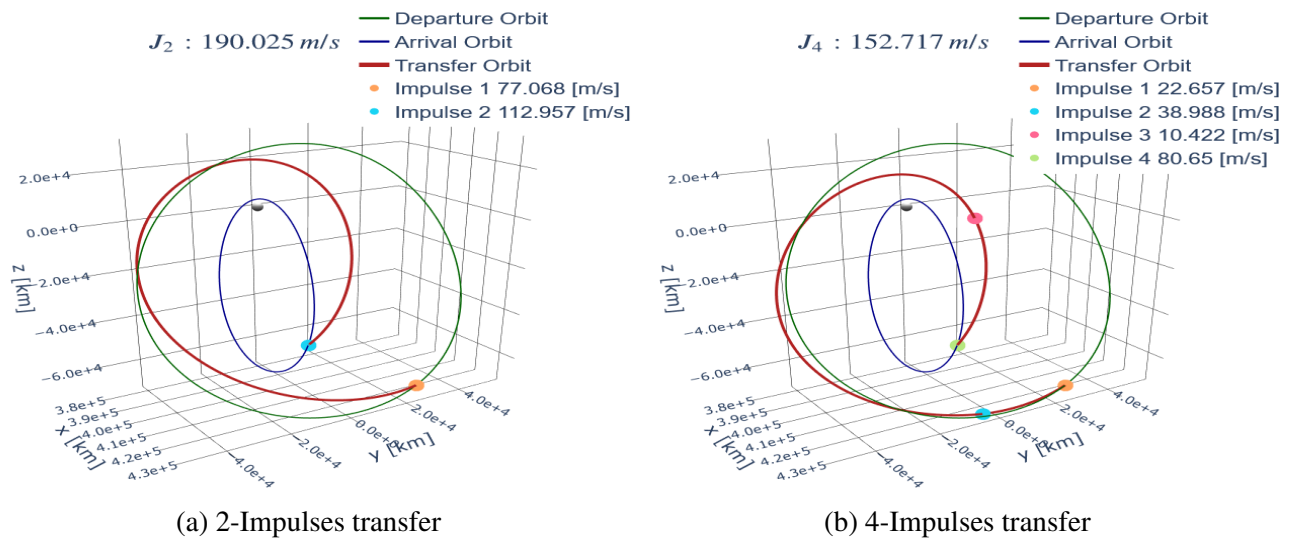


Figure 9: L_2 southern Halo to Gateway transfer: $T_d = 2 T_a$, $\theta_d = 150^\circ$, $\theta_a = 110^\circ$

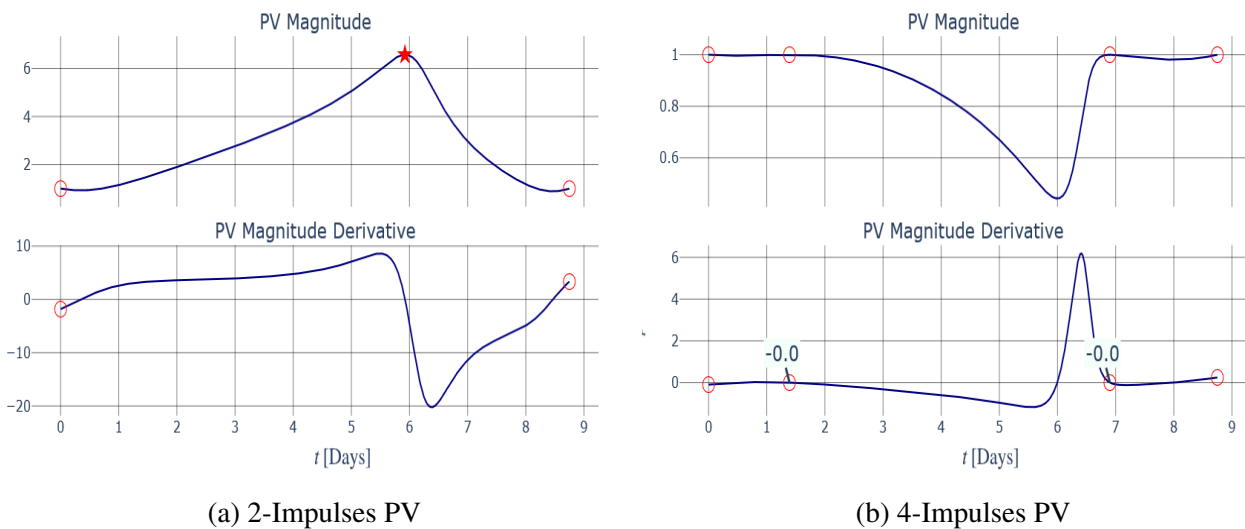


Figure 10: L_2 southern Halo to Gateway PV: $T_d = 2 T_a$, $\theta_d = 150^\circ$, $\theta_a = 110^\circ$

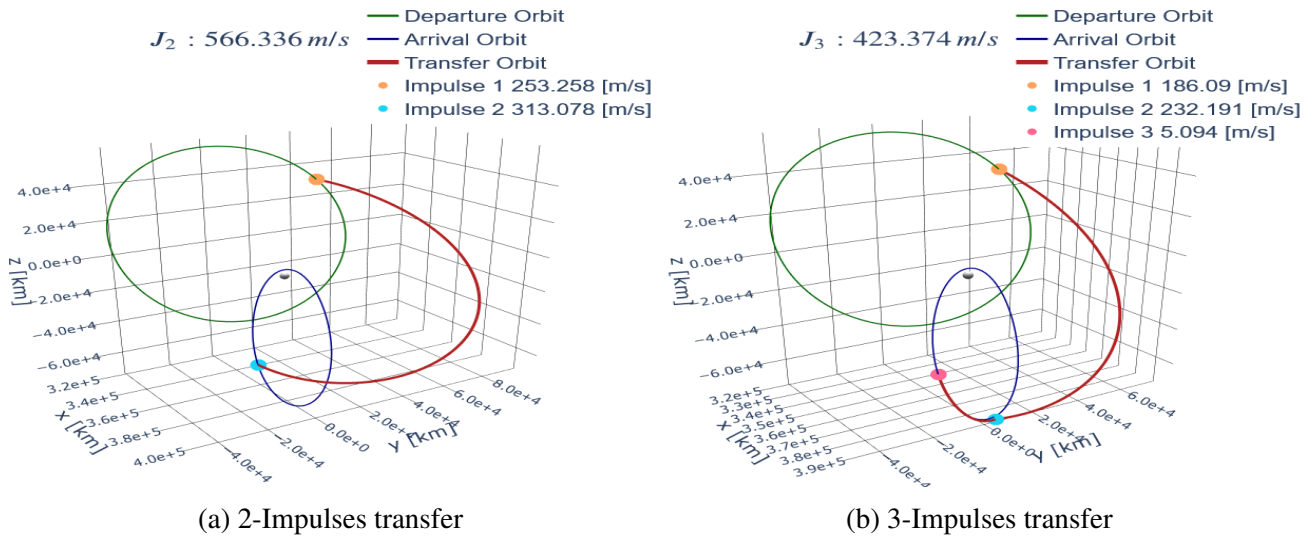


Figure 11: L_1 northern Halo to Gateway transfer: $C_d = C_a$, $\theta_d = 250^\circ$, $\theta_a = 300^\circ$

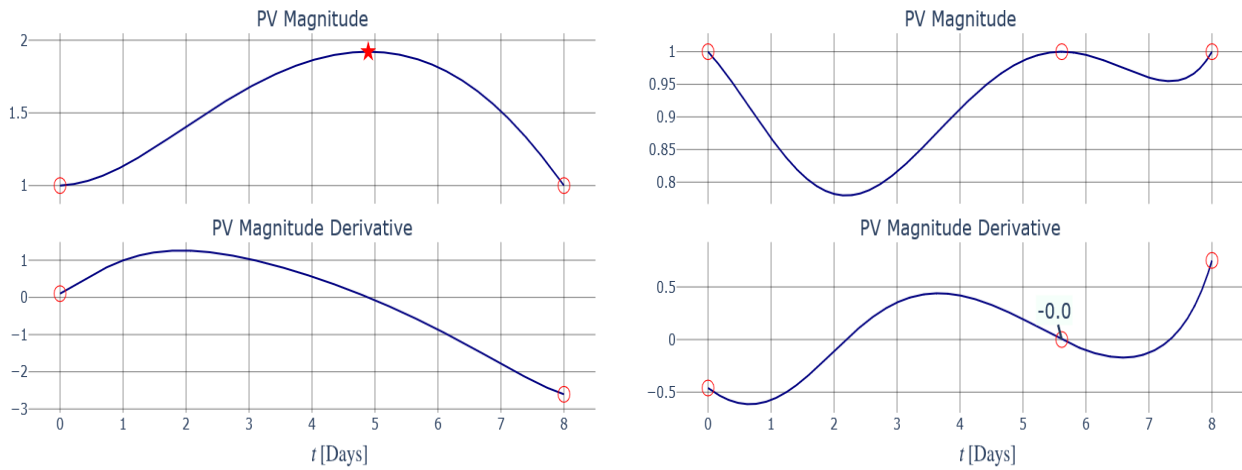


Figure 12: L_1 northern Halo to Gateway PV: $C_d = C_a$, $\theta_d = 250^\circ$, $\theta_a = 300^\circ$

5 CONCLUSION

A high-thrust optimization algorithm for fixed-time orbital transfers in CR3BP environment was proposed via a rigorous and sequential formulation. It consists of a multi-maneuvers guidance for fuel consumption minimization, characterized by multiple intermediate thrusts with positions and times determined in accordance with a non-linear optimization process based on PV theory. The simulations showed the potentiality of the present optimization algorithm, both as tool for generic studies in mission design analysis and as first step for future on-board autonomous Guidance. More specifically, the method has evidenced some points of strength and weakness that it is worthy to emphasize.

The main advantage brought by the algorithm described in this work is probably the possibility to design optimal trajectories with notable fuel saving. Significant decreases in the propellant consumption are generally obtainable, aspect that can help improve the efficiency of future Moon missions and make them more repeatable in this epoch of high interest in space. Another positive feature is the relative ease in the implementation, given that the core of the whole process consists of a gradient-based optimization exploiting the well-consolidated PV theory.

On the other hand, there are some evident drawbacks that must be assessed separately in possible future investigations. First of all, the optimization relies on the effectiveness of nested numerical

procedures, such as the Multiple Shooting and the 2-impulses initial guess determination method, the convergence of which is fundamental to ensure good performance. Furthermore, up to date no work has been carried out in the literature related to this topic around the possible extension of PV theory to more accurate dynamic models (like the N-body problem, a more accurate non-uniform gravity model for the Earth, etc.). Lastly, more simulations should be run in order to effectively prove the algorithm's extendibility to a large variety of case scenarios. At the moment, unfortunately, it is difficult to carry out such tests, given that the more the distance between the orbits involved, the more difficult it is, in sense of numerical convergence, to compute a reasonable initial guess and consequently the lower the performance of the optimization process. Future investigations should focus on studying these aspects deeper in order to validate the current algorithm and hopefully make improvements to it.

REFERENCES

- [1] M. Smith, D. Craig, N. Herrmann, *et al.*, “The artemis program: An overview of nasa’s activities to return humans to the moon,” in *2020 IEEE Aerospace Conference*, IEEE, 2020, pp. 1–10.
- [2] G. Chavers, N. Suzuki, M. Smith, *et al.*, “Nasa’s human lunar landing strategy,” in *International Astronautical Congress*, 2019.
- [3] E. M. Zimovan, K. C. Howell, and D. C. Davis, “Near rectilinear halo orbits and their application in cis-lunar space,” in *3rd IAA Conference on Dynamics and Control of Space Systems, Moscow, Russia*, vol. 20, 2017, p. 40.
- [4] L. R. Capdevila and K. C. Howell, “A transfer network linking earth, moon, and the triangular libration point regions in the earth-moon system,” *Advances in Space Research*, vol. 62, no. 7, pp. 1826–1852, 2018.
- [5] K. Oshima, “The use of vertical instability of l_1 and l_2 planar lyapunov orbits for transfers from near rectilinear halo orbits to planar distant retrograde orbits in the earth–moon system,” *Celestial Mechanics and Dynamical Astronomy*, vol. 131, no. 3, p. 14, 2019.
- [6] H. Curtis, *Orbital mechanics for engineering students*. Butterworth-Heinemann, 2013.
- [7] W. Qiu-Dong, “The global solution of the n-body problem,” *Celestial Mechanics and Dynamical Astronomy*, vol. 50, pp. 73–88, 1990.
- [8] S. Ross, W. Koon, M. Lo, and J. Marsden, *Dynamical Systems, the Three-Body Problem, and Space Mission Design*. Apr. 2011, ch. 2, ISBN: 978-0-615-24095-4.
- [9] C. Zhang, F. Topputo, F. Bernelli-Zazzera, and Y.-S. Zhao, “Low-thrust minimum-fuel optimization in the circular restricted three-body problem,” *Journal of Guidance, Control, and Dynamics*, vol. 38, no. 8, pp. 1501–1510, 2015.
- [10] J. T. Betts, “Survey of numerical methods for trajectory optimization,” *Journal of guidance, control, and dynamics*, vol. 21, no. 2, pp. 193–207, 1998.
- [11] J. M. Longuski, J. J. Guzmán, and J. E. Prussing, *Optimal control with aerospace applications*. Springer, 2014.
- [12] D. F. Lawden, *Optimal trajectories for space navigation*. Butterworths, 1963, vol. 3.
- [13] R. P. Russell, “Primer vector theory applied to global low-thrust trade studies,” *Journal of Guidance, Control, and Dynamics*, vol. 30, no. 2, pp. 460–472, 2007.

- [14] G. Bucchioni, G. Gemignani, F. Lombardi, *et al.*, “Optimal time-fixed impulsive non-keplerian orbit to orbit transfer algorithm based on primer vector theory,” *Communications in Nonlinear Science and Numerical Simulation*, p. 107 307, 2023.
- [15] E. Blazquez, T. Gateau, and S. Lizy-Destrez, “Sempy: A python open-source toolbox for non-keplerian astrodynamics,” in *International Conference on Astrodynamics Tools and Techniques (ICATT)*, 2021.
- [16] K. A. Bokelmann and R. P. Russell, “Optimization of impulsive europa capture trajectories using primer vector theory,” *The Journal of the Astronautical Sciences*, vol. 67, no. 2, pp. 485–510, 2020.
- [17] D. L. Richardson, “Analytic construction of periodic orbits about the collinear points,” *Celestial mechanics*, vol. 22, no. 3, pp. 241–253, 1980.
- [18] B. A. Conway, *Spacecraft trajectory optimization*. Cambridge University Press, 2010, vol. 29.
- [19] D. J. Jezewski and H. L. Rozendaal, “An efficient method for calculating optimal free-space n-impulse trajectories.,” *AIAA journal*, vol. 6, no. 11, pp. 2160–2165, 1968.
- [20] S. Wright, J. Nocedal, *et al.*, “Numerical optimization,” *Springer Science*, vol. 35, no. 67-68, p. 7, 1999.
- [21] S. N. Ha, “A nonlinear shooting method for two-point boundary value problems,” *Computers & Mathematics with Applications*, vol. 42, no. 10-11, pp. 1411–1420, 2001.
- [22] A. Ranganathan, “The levenberg-marquardt algorithm,” *Tutorial on LM algorithm*, vol. 11, no. 1, pp. 101–110, 2004.
- [23] *Sempy-user*, <https://gitlab.isae-superaero.fr/sempy/sempy-user>, Accessed: 23 May 2023.
- [24] R. P. Russell, “On the solution to every lambert problem,” *Celestial Mechanics and Dynamical Astronomy*, vol. 131, no. 11, p. 50, 2019.
- [25] R. Pritchett, K. Howell, and D. Grebow, “Low-thrust transfer design based on collocation techniques: Applications in the restricted three-body problem,” Aug. 2017.
- [26] J. Williams, D. Lee, R. Whitley, K. Bokelmann, D. Davis, and C. Berry, “Targeting cislunar near rectilinear halo orbits for human space exploration,” Feb. 2017.
- [27] *Numpy.gradient*, <https://numpy.org/doc/stable/reference/generated/numpy.gradient.html>, Accessed: 25 May 2023.
- [28] G. Bucchioni, S. Lizy-Destrez, T. Vaujour, V. Thoraval, L. Rouverand, and C. Silva, “Phasing with near rectilinear halo orbits: Design and comparison,” *Advances in Space Research*, vol. 71, no. 5, pp. 2449–2466, 2023.